Optical parametric amplification of 1-kHz high-energy picosecond midinfrared pulses and application to infrared transient-grating experiments on diamond

A. Tokmakoff, C. D. Marshall,* and M. D. Fayer

Department of Chemistry, Stanford University, Stanford, California 94305

Received October 29, 1992; revised manuscript received March 8, 1993

Optical parametric generation of high-repetition-rate high-energy picosecond mid-IR pulses is demonstrated by use of a Q-switched mode-locked cavity-dumped output-coupled Nd:YAG laser as the pump source for a seeded $LiIO_3$ optical parametric amplifier. By mixing a high-energy cavity-dumped pulse that is frequency doubled to $\lambda = 532$ nm with a dye-laser pulse at $\lambda = 611$ nm, we generated 2-μJ, 50-ps pulses at $\lambda = 4.1$ μm at a repetition rate of 1 kHz. The application of these IR pulses to nonlinear spectroscopy is demonstrated by measurement of the thermal diffusivity of diamond with IR transient-grating experiments.

INTRODUCTION

Recent advances in nonlinear-optical materials and high-power pump sources have generated a surge of interest in the generation of short IR pulses in optical parametric devices. Generation of near-IR femtosecond pulses has been demonstrated with optical parametric oscillators that use $KTiOPO_4$ (KTP)[1–3] and $LiNbO_3$ (Ref. 4) as well as with multipass optical parametric amplification in β-BaB_2O_4 (BBO).[5] Subpicosecond pulses in the mid-IR region have been generated by optical parametric amplification in $LiNbO_3$ (Ref. 6) and $LiIO_3$.[7,8] Picosecond IR pulses have been generated by use of various optical parametric schemes. A wide range of wavelengths has been covered by using materials including BBO (0.4–2 μm),[9,10] LBO (0.4–2.6 μm),[11–13] KTP (0.4–4.0 μm),[14,15] $LiNbO_3$ (1.4–4.5 μm),[16–19] $LiIO_3$ (3.5–5.4 μm),[6,20–22] and $AgGaS_2$ (1.2–10 μm).[23–25]

Particular progress in optical parametric devices has been made in the wavelength region of 1.2–1.6 μm, where reliable high-power high-repetition-rate lasers are of great technological interest. Yet wavelengths longer than 3 μm are of particular interest for vibrational spectroscopies, chemical-reactivity experiments, and condensed-matter studies. Generation of short IR pulses in this regime has been demonstrated to yield high repetition rate[23] or high peak power[20,24,26] but not both, as is desirable for nonlinear spectroscopies. For time-domain four-wave mixing experiments and other nonlinear spectroscopies it is vital to have both the peak power to generate a detectable signal and a high repetition rate to permit signal averaging of complex decays on reasonable time scales. To bridge this gap optical parametric amplification techniques involving the mixing of regeneratively amplified frequency-doubled Nd:YAG pulses with amplified dye-laser pulses in $LiIO_3$ have been developed.[21,22] This method of generating $\sim 10^2$-nJ energies involves extensive optical manipulation and requires much costly laser equipment.

In this paper we present a mixing scheme for generation of high-energy picosecond mid-IR pulses at kilohertz repetition rates by use of a seeded $LiIO_3$ optical parametric amplifier (OPA). We describe the generation of 2-μJ pulses at 4.1 μm in detail. We demonstrate the use of these pulses for nonlinear-optical experiments in the IR by measurement of the thermal diffusivity of diamond with transient-grating experiments. To the best of our knowledge this is the first example of a transient-grating experiment in the mid-IR.

The picosecond laser system that we used to pump the OPA is based on a Q-switched mode-locked cavity-dumped output-coupled Nd:YAG laser. This laser has the advantage of being able to pump a dye laser and to dump a high-energy (2-mJ) 100-ps pulse simultaneously for use in pumping amplification components. This Nd:YAG resonator thus serves as both a mode-locked dye-laser pump source and a multipass regenerative amplifier. The dual output renders this laser, when coupled with a synchronously pumped cavity-dumped dye laser, very useful as a high-peak-power seeded OPA pump source when pulse durations of tens of picoseconds are sufficiently short for experimental application. This mixing technique is demonstrated at a repetition rate of 1 kHz, although we have previously run the laser to as high as 2.25 kHz. Even though this laser is demonstrated by generation of pulses at 4.1 μm, one can use the same laser system, with different nonlinear crystals, for difference- and sum-frequency mixing of high-energy picosecond pulses from the UV to 10 μm.

GENERATION OF PICOSECOND MIDINFRARED PULSES

One accomplishes the optical parametric generation of mid-IR light by difference-frequency mixing a high-energy frequency-doubled Nd:YAG pump pulse with a 611-nm dye-laser idler pulse in $LiIO_3$ to generate the signal pulse at 4.1 μm. The pump source of the OPA is a Q-switched mode-locked cavity-dumped output-coupled Nd:YAG laser. The output-coupled pulse train synchronously pumps a cavity-dumped dye laser, which forms the idler pulse. The

0740-3224/93/091785-07$06.00

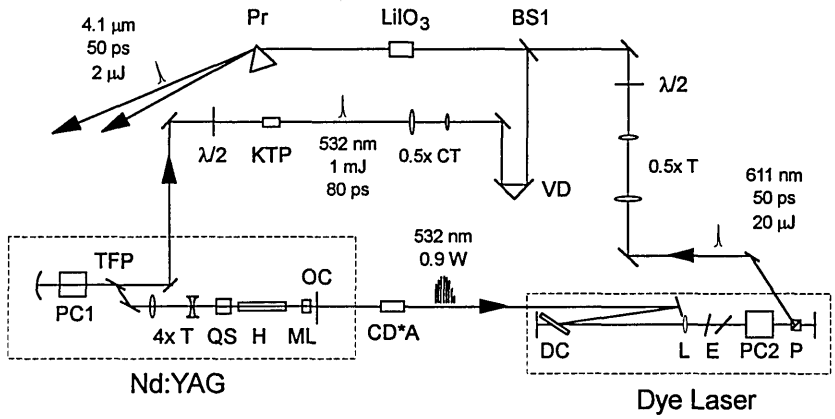

Fig. 1. Seeded $LiIO_3$ OPA pumped by a *Q*-switched mode-locked cavity-dumped output-coupled Nd:YAG–dye-laser combination. BS1, dichroic beam splitter; CT, cylindrical telescope; DC, dye cell; E, solid étalons; H, Nd:YAG head; L, lens; ML, mode locker; OC, output coupler; P, cube polarizer; PC1, PC2, Pockels cells; Pr, prism; QS, *Q* switch; T, telescope; TFP, thin-film polarizer; VD, variable delay; λ/2, half-wave plate.

Nd:YAG is simultaneously cavity dumped with the dye laser and is frequency doubled to create the pump pulse. The pump and idler are made time coincident and collinear and are mixed in a 30-mm $LiIO_3$ crystal.

The cavity-dumped laser is based on a laser that has been described previously[27] and is shown in Fig. 1. The plano-concave cavity is formed by a flat 10% output coupler (OC) and a high reflector with a 200-cm radius of curvature. A thin-film dielectric polarizer inserted into the cavity, with a mirror, as a Brewster-angle jog permits a $LiNbO_3$ Pockels cell to dump a pulse. The gain medium, a 3 mm × 80 mm Nd:YAG rod, is positioned 49 cm from the OC. A 41-MHz mode locker and a *Q* switch are placed 3 and 77 cm, respectively, from the OC. One runs the *Q* switch at a 1-kHz repetition rate in a prelasing mode. The prelasing level, optimized for a balance between power and pulse length, is set for relaxation oscillations beginning 300 μs before the *Q* is switched. One accomplishes cavity-length adjustment by translating the curved cavity mirror.

With these elements alone, the $LiNbO_3$ crystal in the Pockels cell suffers photorefractive damage of the order of 10^5–10^6 s. To minimize this effect, we inserted a 5× Galilean telescope into the cavity. The telescope is constructed of two antireflection-coated fused-silica lenses with $f = -23$ cm and $f = 114$ cm placed 84 and 127 cm, respectively, from the OC. This lens separation gives the maximum filling of the rod by the TEM_{00} mode, permitting the resonator to lase in this mode without an iris. With this telescope, the spot size at the Pockels cell, positioned next to the curved high reflector, was measured as 3.2 mm.

The Pockels cell is a 9 mm × 9 mm × 25 mm $LiNbO_3$ crystal mounted in a *Q*-switch housing. A fast photodiode monitoring the leakage out of the curved high reflector triggers the driver circuit. The high voltage is switched by a vertical field effect transistor (VFET) driver circuit.[28] A double-channel configuration is used to reduce piezoelectric ringing in the $LiNbO_3$. The first board drops one electrode to ground, applying the quarter-wave voltage. After the double pass of the pulse through the Pockels cell the second electrode drops to ground, returning the electric field across the cell to zero. The electrodes recharge slowly between shots. This driver circuit has been run to repetition rates of 8 kHz.

The 1-kHz output of the Nd:YAG is 1.7 W of 1.06 μm in a 250-ns pulse train at the OC without cavity dumping and 1.8 W in the cavity-dumped pulse. These numbers reflect nominal powers during mixing, since the cavity-dumped pulse is picked out at a point substantially past the peak of the pulse train. We obtained powers of 3.0 W in both the full pulse train and the cavity-dumped pulse, but they do not necessarily reflect the optimum conditions for mixing, as discussed below. The stability of the laser intensity is typically ±5% rms, mainly because of 180-Hz power-supply ripple. Both output beams converge slightly, and thus one can efficiently frequency double the beams without further focusing. The pulse train is frequency doubled immediately after the OC in a 4 mm × 4 mm × 25 mm CD*A crystal. The doubled pulse train (0.9 W) is separated from the remaining 1.06-μm output by use of a dichroic beam splitter and then used to pump the dye laser. The cavity-dumped pulse is doubled in a 3 mm × 3 mm × 5 mm KTP crystal, 200 cm beyond the thin-film polarizer, giving a 1-mJ, 80-ps pulse (FWHM) at 532 nm. A half-wave plate placed in front of the KTP crystal acts as an attenuator without changing the heating of the crystal, whereas the angle of the crystal fixes the polarization for mixing.

The OC pulse train synchronously pumps an acid-shifted Sulforhodamine-640 dye laser at $\lambda = 611$ nm for generation of $\lambda = 4.1$ μm. Wavelengths near 5 μm require that one use Rhodamine B as the dye, and DCM dye is used for wavelengths near 3 μm. The dye-laser cavity, shown in Fig. 1, is formed by two planar high reflectors and an antireflection-coated, $f = 100$ cm lens positioned 96 cm from one end mirror. At this end mirror, a 4-mm dye cell is placed at Brewster's angle to the dye beam path, and the pump beam is focused into the cell in a nearly collinear geometry. The dye bandwidth limitation and tuning are accomplished by use of two matched 100-μm, $R = 70\%$, solid étalons. The laser is cavity dumped by use of a double-crystal KDP Pockels cell and a cube polarizer.

As the Gaussian pulse train pumps the dye laser, the dye pulse train builds in intensity. At the peak of the dye pulse, the dye laser and Nd:YAG laser are simultaneously cavity dumped. The dye-laser output is 20 μJ in 50 ps (FWHM) at 611 nm and is stable to ±5% rms. The dye beam is downcollimated to 1 mm diameter (1/*e*). The 532-nm pump pulse is cylindrically downcollimated to a

1 mm × 2 mm beam. The pulses were made collinear with a dichroic beam splitter and time coincident by variation of the pump-pulse path length. One mixes the beams in a 9 mm × 9 mm × 30 mm $LiIO_3$ crystal cut 22.5° off the optic axis for type-I (*ooe*) mixing. The input face of the crystal is antireflection coated for visble wavelengths. The beams are combined in the crystal so that the 532-nm beam walks off in the long direction of the cylindrical spot, maximizing the interaction length with the dye beam. The input energies at the crystal for the pump and idler beams are 500 and 15 μJ, respectively.

The mid-IR output energy of the OPA at the crystal, measured behind a 3-mm Ge flat is 2 μJ at $\lambda = 4.1$ μm. A cross correlation of the dye pulse with the 4.1-μm by sum-frequency generation in another $LiIO_3$ crystal gave a Gaussian response identical to the dye autocorrelation, implying a 50-ps (FWHM) pulse width. The stability of the 4.1 μm is typically ±10% rms, following the product of the pump and dye stabilities. We did not directly observe the mode quality of the mid-IR light; however, observations by use of irises and slits in front of an integrating sphere with a PbSe detector show that the beam is Gaussian and is not cylindrically distorted within the limits of the measurement. The mid-IR beam has the same spot size as the dye at the output face of the crystal but diverges rapidly with a confocal parameter of 90 cm.

The intensity of the pump beam at the $LiIO_3$ crystal is near the damage threshold. During attempts to raise the conversion efficiency, we used a circular pump spot of 1.5 mm (1/*e*) and a 532-nm pump input energy of 800 μJ at the crystal. The output of the OPA was ~6 μJ at 4.1 μm. This mixing scheme worked for ~1 h, but then the crystal shattered from damage initiated at the input surface. This damage apparently began with damage to the coating on the input face, yet the peak intensity of ~1 GW/cm^2 is similar to previously reported $LiIO_3$ damage thresholds for picosecond pulses.[29]

A number of attempts were made to improve conversion efficiency. Spot sizes larger than those reported above, even those with much higher energy, gave far worse conversion efficiency, typically yielding <100 nJ. Smaller spot sizes are inaccessible because of the damage threshold. A circularly collimated pump beam of 2 mm and a 1-mm dye beam yielded ~200 nJ. A crystal length of 30 mm is sufficient to cause significant walk-off problems because the birefringence angle for these wavelengths is $\rho = 3.1°$, corresponding to a walk-off of $\delta = 1.6$ mm across the crystal. The cylindrical collimation mentioned above minimizes the loss that results from walk-off while maximizing the intensity. Dispersion in such a long crystal should not cause problems because the calculated acceptance bandwidth for the dye beam is 1 cm^{-1}, or 15 ps for transform-limited pulses. With an uncoated 10-mm crystal and identical input parameters, the mid-IR output was 0.3 μJ. For both crystals, the conversion efficiency was approximately linear in both the pump- and the dye-beam intensities. Adjustment of the angles for the input beams demonstrated that the highest conversion efficiency is nearly collinear.

Separation of the pump, idler, and signal beams poses a significant problem. A 3-mm Ge flat properly separates the visible from the IR but is damaged by the pump beam after prolonged exposure. ZnSe dichroic beam splitters offer reasonable separation at a high cost. We chose a CaF_2 Brewster prism to separate the beams in this case. The dispersive properties of CaF_2 are not sufficient to separate the visible colors properly, but they adequately separate the 4.1-μm beam from the visible. The use of a prism also permits the recovery of the visible beams for use in the experiment.

The parameters described above by no means delineate the limits of the apparatus but are appropriate for the experiments described below. The values quoted for the pulse duration are not optimal inasmuch as only a low-quality mode locker was available. With the use of a better mode locker we expect an improvement in both the mid-IR pulse length and the conversion efficiency. The pulse lengths expected for this laser are 60 ps for the 532-nm cavity-dumped beam and 20 ps for the dye pulse length. Note that, for mid-IR generation at 5 μm, one would use Rhodamine B dye, which has been demonstrated to give 25-ps, 40-μJ pulses for similar pump characteristics with this dye laser. These dye pulse characteristics would certainly decrease pulse length without altering the mid-IR energy. If pulse length is a prime concern, a dye pulse can be selected later in the dye pulse train. We observed that the dye-laser pulse length decreased by ~4 ps/pulse in the tail of the pulse train, but the output energy drops off quickly. In addition, higher IR pulse energies may be obtained by use of different amplification schemes involving multipass or multiple-crystal arrangements as have been demonstrated by others.[5,9–11] Although this system was demonstrated for a repetition rate of 1 kHz, an identical cavity-dumped Nd:YAG laser has been run up to 2.25 kHz with little degradation in the output energies. One can improve the stability of the mid-IR pulses with a better Nd:YAG laser power supply, considering the nonlinear relationship between the mid-IR and the Nd:YAG fundamental intensities.

Generation of picosecond mid-IR pulses by use of the cavity-dumped Nd:YAG–dye laser combination described above is not limited to the mixing scheme described above. Generation of mid-IR pulses beyond 5 μm, by difference-frequency mixing in $AgGaS_2$, is performed with a similar dual-crystal mixing scheme. As set forth above, we created mid-IR pulses by frequency doubling $\lambda = 1.06$ μm in KTP and then difference-frequency mixing $\lambda = 532$ nm with a dye pulse in $LiIO_3$. Similarly, a 1.06-μm pulse could be difference-frequency mixed with a dye pulse ($\lambda = 592$–560 nm) in KTP to give near-IR picosecond pulses ($\lambda = 1.19$–1.34 μm). These near-IR pulses can be mixed again with 1.06 μm in $AgGaS_2$ to yield 5–10-μm picosecond pulses.[24,30] The same scheme will work with $LiIO_3$ when one desires wavelengths that are shorter than 5.3 μm.[31]

This apparatus can also be used to generate picosecond pulses in the blue and UV through sum-frequency generation. One can generate blue wavelengths by mixing the $\lambda = 1.06$ μm cavity-dumped pulse with an IR dye pulse. One can easily reach UV wavelengths by mixing the frequency-doubled Nd:YAG laser with a dye. In the wavelength region in which visible dyes operate effectively one can use the cavity-dumped output for amplification of the dye output to ~100 μJ.

Clearly, the cavity-dumped Nd:YAG–dye-laser combination is an excellent pump laser for a picosecond-seeded

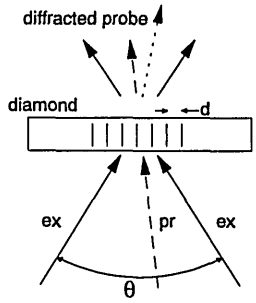

Fig. 2. Schematic of the IR transient-grating experiment. Two $\lambda = 4.1$ μm excitation pulses (ex) are crossed at an angle θ in the diamond. Absorption and rapid relaxation by the two-phonon bands create a thermal grating with fringe spacing d. The diffraction of a variably delayed probe pulse (pr) monitors the decay of the grating by thermal diffusion from the peaks to the nulls.

OPA. By varying mixing schemes, one can use it to generate any IR wavelength to 10 μm. Other features make it a useful source for many experiments. The system provides a combination of reasonably high repetition rate (1 kHz), reasonably short pulses ($\leq$50 ps), and high energy (2 μJ). This is accomplished by use of a single Nd:YAG laser and a simple dye laser, which renders the system inexpensive compared with methods that involve the use of a multipass regenerative amplifier to amplify synchronously pumped dye-laser pulses and to pump the OPA.

TRANSIENT-GRATING EXPERIMENTS WITH PICOSECOND MIDINFRARED PULSES

Picosecond IR pulses are of considerable interest for the study of numerous physical and chemical systems. A picosecond IR source opens the doors for dynamic studies of molecular-vibrational phenomena in gas and condensed phases, chemical reactivity and bonding, and microscopic and bulk phenomena in condensed phases. High-energy and high-repetition-rate picosecond pulses are most useful in nonlinear-optical experiments. As an application of the capability of picosecond IR pulses to perform nonlinear-optical experiments, we demonstrate the measurement of the high thermal diffusivities of natural and isotopically enriched type-IIA diamond by use of IR transient-grating experiments with a visible probe.[32]

The measurement of extremely large thermal conductivities such as those of diamond is difficult. Traditional steady-state measurement techniques require contact with the sample and are limited by the size of the sample.[33,34] Modulated laser heating techniques require complex models describing the phase or amplitude of thermal waves.[35,36] Measurements of transient IR signals after pulsed heating have provided the most direct measurements to date, but in most cases they are also limited by the size of the sample and the description of the thermal wave.[37,38]

The transient grating is an entirely optical technique; it is noninvasive, direct, and requires no modeling. Sample-size limitations are dictated only by the spot size of the beam. The experiment directly probes the bulk of the sample on a small-distance scale and is not influenced by surface effects. In addition, this technique has internal consistency checks that permit verification of the results.

The transient-grating experiment is shown in Fig. 2. Two time-coincident picosecond 4.1-μm pulses are crossed in the diamond sample at an angle θ. The two beams produce a sinusoidal interference pattern in the sample with a fringe spacing of $d = \lambda/2 \sin(\theta/2)$. Absorption of the IR light by the two-photon modes in diamond[39] deposits heat into the sample in a pattern mimicking the original optical interference pattern. The spatially periodic heating of the sample ($\Delta T \approx 0.1$ K) causes a spatial modulation of the real part of the index of refraction. This produces a diffraction grating. A third, time-delayed probe pulse, obtained from the dye beam, is diffracted off the grating at the Bragg angle. The probe monitors the decay of the grating as heat diffuses from the peaks to the nulls. One can obtain the probe diffraction efficiency η by solving a one-dimensional diffusion relation[40]:

$$\eta \propto \exp(-2\alpha\beta^2 t) = \exp(-t/\tau), \tag{1}$$

where $\beta = 2\pi/d$ is the grating wave vector and $1/\tau$ is the measured grating-decay constant. The factor of 2 arises because the signal intensity in this four-wave mixing experiment is proportional to the square of the induced polarization. Relation (1) shows that the measured exponential grating-decay time gives the thermal diffusivity directly from $\alpha = (-2\beta^2\tau)^{-1}$. An accurate test of the diffusive nature of the decay is to vary the grating fringe spacing. This changes the grating wave vector and the experimental decay time, but the thermal diffusivity remains the same.

Transport of the 4.1-μm beam to the experiment is shown in Fig. 3. The beam is expanded and collimated to a 6.5-mm-diameter beam with a 4$\times$ expanding telescope 50 cm from the $LiIO_3$ crystal. The mid-IR beam is made collinear with a He–Ne laser beam of the same spot size by use of a ZnSe dichroic beam splitter. PbSe position-sensitive detectors, which detect both the He–Ne beam and the mid-IR beam, are placed behind the beam splitter and at a pick-off point farther down the beam. Centering both beams on each detector ensures their exact collinearity. The mid-IR beam is split into two excitation beams with a ZnSe beam splitter, and it is focused and is crossed at the sample by use of a gold 114-mm off-axis parabolic reflector. This permits the IR beam and the collinear He–Ne laser beam to focus at the same position, which simplifies sample alignment, crossing of the beams, and location of the signal. Since the beams are parallel when brought into the parabolic reflector, one changes the fringe spacing by changing their separation.

The dye beam is recovered after the dispersing prism for use as the probe pulse. Since both the pump and the dye pulses are approximately collinear, one uses a polarizer to separate the two. The dye beam is spatially filtered and is sent through a double-passed optical-delay line, permitting a delay of up to 16 ns after the excitation pulses. To vary the spot size of the visible probe at the sample, one can use a flat mirror and a separate lens in place of the parabolic reflector.

The experimental setup shown in Fig. 3 shows the configuration for a transient-grating experiment with visible probe. Note that one can use this configuration as is or with minor modification to accommodate a wide variety of linear and nonlinear time-domain spectroscopies with

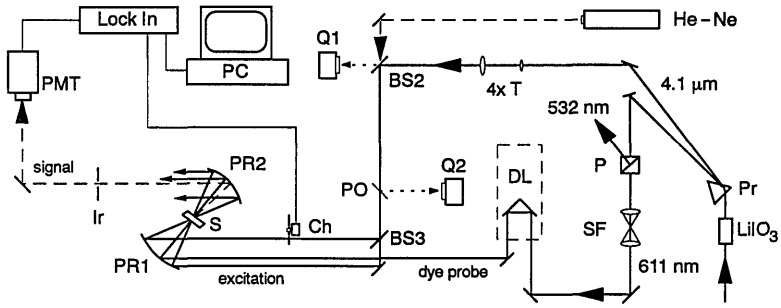

Fig. 3. Beam transport and experimental setup for picosecond IR transient grating. BS2, BS3, beam splitters; Ch, chopper; DL, long optical-delay line; Ir, iris; P, polarizer; PMT, photomultiplier tubes; PO, pick-off; PR1, PR2, off-axis parabolic reflectors; Pr, prism; Q1, Q2, position-sensitive detectors; SF, spatial filter; T, telescope.

both IR and visible pulses, such as pump–probe experiments and photon echoes. In addition, one can employ either of the visible beams for frequency-upconversion detection of IR signals.

The mid-IR and dye beams are focused to 150 and 100 μm, respectively, at the sample. The 3-in. (7.62-cm) parabolic reflector permits variation of the fringe spacing from 11 to 21 μm. The transmitted beams and the signal are recollimated by a second parabolic reflector. This permits the transient-grating signal to be found quickly relative to the transmitted He–Ne beams even when the signal is invisible. The diffracted grating signal is detected by a PMT. The PMT signal is detected with a lock-in amplifier while chopping one excitation beam at half the repetition rate.

The grating fringe spacing is determined by the acoustic-grating signal from a sample of 10% deuterated ethanol in ethanol. The excitation pulses are absorbed by the deuterated-ethanol hydrogen-bonded O—D stretching mode, which rapidly relaxes (~1 ps) into phonon modes. This rapid heating launches counterpropagating acoustic waves, with a wavelength equal to the grating fringe spacing.[41] Since the thermal decay is slow relative to the acoustic period, the grating signal probes the density modulations as the acoustic waves travel against each other at the speed of sound. One can accurately determine the fringe spacing by fitting the acoustic grating signal to the speed of sound in ethanol. Because the acoustic signal from ethanol is easily discernible by the eye even under bright room lights, it is also useful for visually lining up the transient-grating signal into the PMT. The transient-grating signal from diamond, although too weak for one to see, follows nearly the same path.

Thermal-diffusivity measurements were made on two type-IIA, 4 mm × 4 mm × 0.5 mm synthetic-diamond samples. One sample had a ^{12}C isotopic concentration of 98.9%, corresponding to the natural abundance, and the other had a 99.9% ^{12}C concentration. A typical transient-grating signal decay for each sample at a fringe spacing of 11.8 μm is shown in Fig. 4(a). The thermal-grating decays are exponential over several factors of e and are also modulated by counterpropagating acoustic waves. One separates the acoustic signal by subtracting the exponential fit to the thermal portion from the signal, taking into account the quadratic dependence of the signal. The difference can then be fitted to an exponentially damped sinusoidal signal, as shown in Fig. 4(b). The velocity of sound in diamond, v, determined by the average to several fits, was $v = 1.73 \times 10^6$ cm/s, corresponding to literature values within 2%.[42]

The quality of the data collected by use of this apparatus is clear from Fig. 4. The high energy per pulse is vital considering the diffraction efficiency of $\sim 10^{-5}$ for this particular experiment. The high repetition rate permits scans such as those shown in Fig. 4 to be averaged in <10 min.

Measurements of the thermal diffusivity on any spot on the sample were reproducible to within ±1%. However, the thermal-diffusivity measurements on both samples varied significantly from point to point over the entire sample. Measurements were made at many points on each sample, giving thermal-diffusivity values that varied by as much as 50% from point to point. The local variations of the thermal diffusivity are not surprising when one compares results with x-ray topographs of the samples. X-ray topogaphs of the samples used in this experiment, published elsewhere,[43] show considerable defect structures of the order of ≤50 μm in some regions and relatively few defects in others.

To make a determination of the average thermal diffusivity of the samples, we made measurements for several points and averaged them. This averaging was then repeated for several fringe spacings. Using relation (1), one can obtain a plot of the decay constant versus the square of the grating wave vector; this plot should give a straight line through the origin with slope α. Figure 5 shows such

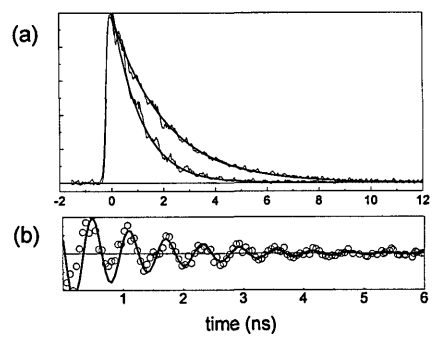

Fig. 4. (a) Two transient-grating decays and exponential fits for natural-abundance ^{12}C (upper curve) and isotopically enriched diamond (lower curve) at a fringe spacing of 11.8 μm. (b) Enlargement of the acoustic portion of the signal for the lower curve in (a), with an exponentially damped sinusoidal fit.

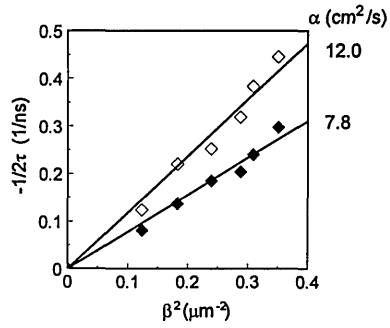

Fig. 5. Plot of the average grating-decay constant versus the square of the grating wave vector at six fringe spacings for both diamond samples. The upper line corresponds to the isotopically enhanced diamond, and the lower line corresponds to the natural-abundance diamond. The intercept at the origin is a check of the diffusive nature of the process.

a plot for fringe spacings of 11.8 to 18.0 μm for both natural-abundance and isotopically enriched diamond. The slope gives the thermal diffusivity of diamond as 7.8 ± 0.2 cm^2/s for 98.9% ^{12}C (natural abundance) and 12.0 ± 0.2 cm^2/s for 99.9% ^{12}C, corresponding to thermal conductivities of 14.0 and 21.5 W/cm K, respectively. These results confirm previous measurements of 50% enhancement in the thermal conductivity of isotopically enhanced single-crystal diamond.[35,44] However, note that the nature of the enhanced thermal conductivity cannot be absolutely assigned to the isotopic purity but may also be due to the defect properties of these particular gems. Further temperature-dependent thermal-diffusivity studies on these diamonds will provide additional information regarding their material properties.

CONCLUDING REMARKS

Optical parametric generation of near-IR wavelengths currently offers the best method of generating picosecond pulses at mid-IR wavelengths. These techniques do not suffer from the unreliability and limited tuning range of color-center lasers and are substantially more accessible than are free-electron lasers. Optical parametric schemes of generating picosecond mid-IR pulses have been limited by either repetition rate or peak power per pulse, as required for many nonlinear spectroscopies. The system described above offers the unique characteristics of high-energy and high-repetition-rate pulses of 50-ps duration over a wide range of IR wavelengths. The fact that the system is based on the dual output of a mode-locked *Q*-switched cavity-dumped output-coupled Nd:YAG laser permits the single resonator to function as both a high-power dye-laser pump source and an amplifying laser. Since the cavity-dumped Nd:YAG–dye-laser combination can be readily adapted to achieve any wavelength from the UV to the mid-IR, it is a versatile tool for a wide variety of spectroscopic applications.

ACKNOWLEDGMENTS

We thank William F. Banholzer of the General Electric Company, Schenectady, New York, for supplying the diamond samples. We also thank Carl C. Reiner of the School of Chemical Sciences, University of Illinois, Urbana-Champaign, Urbana, Illinois, for his help in designing the VFET Pockels-cell-driver circuitry. We also thank Scott Greenfield of the Argonne National Laboratory for his help in developing the position-sensitive-detector electronics and valuable discussions concerning the transport of IR beams. This research was supported by a grant from the National Science Foundation, Division of Materials Research (DMR90-22675), and by a grant from the Office of Naval Research, Physics Division (N00014-89-J1119).

*Permanent address, Lawrence Livermore National Laboratory, Livermore, California 94551.

REFERENCES

1. D. C. Edelstein, E. S. Wachman, and C. L. Tang, Appl. Phys. Lett. **54,** 1728 (1989).
2. G. Mak, Q. Fu, and H. M. van Driel, Appl. Phys. Lett. **60,** 542 (1992).
3. Q. Fu, G. Mak, and H. M. van Driel, Opt. Lett. **17,** 1006 (1992).
4. R. Laenen, H. Graener, and A. Laubereau, Opt. Commun. **77,** 226 (1990).
5. W. Joosen, P. Agostini, G. Petite, J. P. Chambaret, and A. Antonetti, Opt. Lett. **17,** 133 (1992).
6. D. S. Moore and S. C. Schmidt, Opt. Lett. **12,** 482 (1987).
7. T. M. Jedju, L. Rothberg, and A. Labrie, Opt. Lett. **13,** 961 (1988).
8. T. Elsaesser and M. C. Nuss, Opt. Lett. **16,** 411 (1991).
9. U. Sukowski and A. Seilmeier, Appl. Phys. B **50,** 541 (1990).
10. J. Y. Huang, J. Y. Zhang, Y. R. Shen, C. Chen, and B. Wu, Appl. Phys. Lett. **57,** 1961 (1990).
11. H. J. Krause and W. Daum, Appl. Phys. Lett. **60,** 2180 (1992).
12. J. Y. Zhang, J. Y. Huang, Y. R. Shen, C. Chen, and B. Wu, Appl. Phys. Lett. **58,** 213 (1991).
13. M. Ebrahimzadeh, G. J. Hall, and A. I. Ferguson, Opt. Lett. **18,** 278 (1993).
14. H. Vanherzeele, Appl. Opt. **29,** 2246 (1990).
15. M. Ebrahimzadeh, G. H. Hall, and A. I. Ferguson, Opt. Lett. **16,** 1744 (1991).
16. A. Seilmeier, K. Spanner, A. Laubereau, and W. Kaiser, Opt. Commun. **24,** 237 (1978).
17. J. T. Knudson and J. C. Stephenson, Chem. Phys. Lett. **107,** 385 (1984).
18. T. Elsaesser, R. J. Baeuerle, and W. Kaiser, Infrared Phys. **29,** 503 (1989).
19. H. Graener, T. Q. Ye, and A. Laubereau, Chem. Phys. Lett. **164,** 12 (1989).
20. E. J. Heilweil, R. R. Cavanaugh, and J. C. Stephenson, Chem. Phys. Lett. **134,** 181 (1987).
21. M. Iannone, B. R. Cowen, R. Diller, S. Maiti, and R. M. Hochstrasser, Appl. Opt. **30,** 5247 (1991).
22. T. M. Judju, M. W. Roberson, and L. Rothberg, Appl. Opt. **31,** 2684 (1992).
23. A. G. Yodh, H. W. K. Tom, G. D. Aumiller, and R. S. Miranda, J. Opt. Soc. Am. B **8,** 1663 (1991).
24. K. G. Spears, X. Zhu, X. Yang, and L. Wang, Opt. Commun. **66,** 167 (1988).
25. T. Elsaesser, H. Lobentanzer, and A. Seilmeier, Opt. Commun. **52,** 355 (1985).
26. J. D. Beckerle, R. R. Cavanaugh, M. P. Casassa, E. J. Heilweil, and J. C. Stephenson, J. Chem. Phys. **95,** 5403 (1991).
27. V. J. Newell, F. W. Deeg, S. R. Greenfield, and M. D. Fayer, J. Opt. Soc. Am. B **6,** 257 (1989).
28. J. C. Postlewaite, J. B. Miers, C. C. Reiner, and D. D. Dlott, IEEE J. Quantum Electron. **24,** 411 (1988).
29. V. G. Dmitriev, *Handbook of Nonlinear Optical Crystals* (Springer-Verlag, Berlin, 1991).
30. K. Kato, IEEE J. Quantum Electron. **QE-20,** 698 (1984).
31. K. Kato, IEEE J. Quantum Electron. **QE-21,** 119 (1985).

32. A. Tokmakoff, W. F. Banholzer, and M. D. Fayer, Appl. Phys. A **53,** 87 (1993).
33. D. T. Morelli, C. P. Beetz, and T. A. Perry, J. Appl. Phys. **64,** 3063 (1988).
34. T. R. Anthony, J. L. Fleischer, J. R. Olson, and D. G. Cahill, J. Appl. Phys. **69,** 8122 (1991).
35. T. R. Anthony, W. F. Banholzer, J. F. Fleischer, L. Wei, P. K. Kuo, R. L. Thomas, and R. W. Pryor, Phys. Rev. B **42,** 1104 (1990).
36. E. P. Visser, E. H. Versteegen, and W. J. P. van Enckervort, J. Appl. Phys. **71,** 3238 (1992).
37. G. Lu and W. T. Swann, Appl. Phys. Lett. **59,** 1556 (1991).
38. Z. H. Chen and A. Mandelis, Phys. Rev. B **46,** 13,526 (1992).
39. C. A. Klein, T. M. Hartnett, and C. J. Robinson, Phys. Rev. B **45,** 12,854 (1992).
40. C. D. Marshall, I. M. Fishman, R. C. Dorfman, C. B. Eom, and M. D. Fayer, Phys. Rev. B **45,** 10,009 (1992).
41. K. A. Nelson, R. J. D. Miller, D. R. Lutz, and M. D. Fayer, J. Appl. Phys. **53,** 1144 (1982).
42. W. Banholzer, T. Anthony, and R. Gilmore, *New Diamond Science and Technology* (Materials Research Society, Pittsburgh, Pa., 1991), p. 857.
43. T. R. Anthony and W. F. Banholzer, Diamond Relat. Mater. **1,** 717 (1992).
44. D. G. Onn, A. Witek, Y. Z. Qiu, T. R. Anthony, and W. F. Banholzer, Phys. Rev. Lett. **68,** 2806 (1992).